Detection and Identification of Reaction Intermediates in the Photorearrangement of Pyridazine *N*-Oxide: Discrepancies between Experiment and Theory

Jiani Ma,[a] *Brian D. Wagner,* [b,c] *Ming-De Li,*[d] *Yibo Lei,*[a] *David Lee Phillips**[a,d] *and Götz Bucher**[e,f]

[a] Key Laboratory of Synthetic and Natural Functional Molecule Chemistry of Ministry of Education, College of Chemistry and Materials Science, Northwest University, Xi'an, P. R. China

[b] current address: University of Prince Edward Island, Charlottetown, P. E. I., Canada C1A 4P3

[c] Steacie Institute for Molecular Sciences, National Research Council of Canada, Ottawa, Ontario, Canada K1A 0R6

[d] Department of Chemistry, The University of Hong Kong, Pokfulam Road, Hong Kong S.A.R., P. R. China

[e] Department of Chemistry, University of Ottawa, Ottawa, Ontario, Canada K1N 6N5

[f] current address: WestCHEM, School of Chemistry, University of Glasgow, Joseph-Black-Building, University Avenue, Glasgow G12 8QQ, United Kingdom.

*Corresponding Authors Email Addresses: phillips@hku.hk; goetz.bucher@glasgow.ac.uk

Abstract

Photolysis of pyridazine *N*-oxide (PNO) results in the detection of a complex series of transient phenomena. On the ultrafast (fs) timescale, we could detect the decay of the first singlet excited state of PNO, and the formation of a short-lived transient species, that, based on its time-resolved resonance Raman (TR^3) spectrum, we assign to the oxaziridine 1,2-diaza-7-oxa-bicyclo[4.1.0]hepta-2,4-diene. On a longer (hundreds of ns) timescale, this species rearranges to a ring-opened diazo compound, which we have also detected by time-resolved infrared and TR^3 spectroscopy. In addition, we identify 1-oxa-3,4-diazepine as a long-lived species formed in the photochemistry of PNO. This species is formed via its oxirane isomer, which in turn is likely formed directly from the S_1 state of PNO via a conical intersection. The barrier determined experimentally for the decay of 1,2-diaza-7-oxa-bicyclo[4.1.0]hepta-2,4-diene (E_a = (7.1 $\pm$ 0.5) kcal mol^{-1}) is far larger than any barrier calculated by any method that includes dynamic electron correlation, but very close to the barriers calculated at the RHF or CASSCF levels of theory. Many methods (B3LYP, MP2, MP4) fail to give a minimum

structure for 1,2-diaza-7-oxa-bicyclo[4.1.0]hepta-2,4-diene, while M06, M06-2X, MP3, CCSD, or CCSD(T) yield activation energies for its electrocyclic ring opening that are far too small. In addition, we note that several important geometric parameters, both of 1,2-diaza-7-oxa-bicyclo[4.1.0]hepta-2,4-diene and of the transition state of its ring opening reaction clearly have reached no convergence, even at the fully optimized CCSD(T)/cc-pVTZ level of theory. We therefore suggest that the transient species described in this contribution might be excellent test molecules for further development of highly correlated and DFT methods.

Introduction

The photochemistry of heteroaromatic *N*-oxides is only insufficiently understood on the molecular level.[1,2] While a wide variety of different products can be isolated, among them products due to ring expansion, –contraction, and –opening as well as products of deoxygenation, the reaction mechanisms leading to them are mostly speculative. Two types of reactions are distinguished: photodeoxygenation, which is believed to occur generally on the triplet surface, and photorearrangement, which is considered to be singlet state chemistry. For the simplest heterocyclic *N*-oxide, pyridine *N*-oxide **1**, it could be shown that atomic oxygen, O (^{3}P), is formed in modest quantum yield upon 308 nm laser excitation.[3] Understanding the main reaction pathway of photorearrangement, however, is complicated for **1** by the fact that in organic solution essentially only tar is formed, while in basic solution the anion species **4** can be isolated and its formation be monitored (Scheme 1).[4,5] The reaction mechanism has been postulated to proceed via bridged oxaziridine **2** and azoxepine **3**, although diradical and nitrene intermediates have been invoked as well.[1,2,6-8]

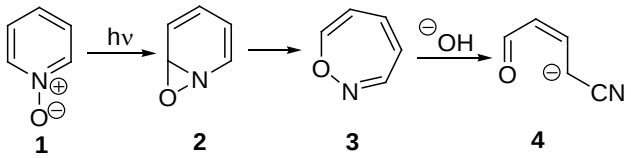

Scheme 1. Reaction sequence postulated for the photolysis of pyridine *N*-oxide **1** in the presence of base

The products of the photochemistry of pyridazine *N*-oxide **5** are better characterized, and although only low yields could be obtained, the formation of furan **13** and cyclopropene-3-carbaldehyde **12** seems to be established.[9] These products point to the intermediate formation of carbene **11**, and hence to the presence of diazo compound **8**, which could again be formed via bicyclic oxaziridine **6** and diazoxepine **7**. Alternatively, an oxygen-walk rearrangement of

6 could yield diazoxepine **10**, via oxirane **9**. In case of a diphenyl-substituted derivative, Tomer et al. were able to monitor the formation of diazo compound **15** upon photolysis of 3,6-diphenylpyridazine *N*-oxide **14** (Scheme 2).[10] An attempt to resolve the growth of **15** by nanosecond laser flash photolysis failed; obviously the formation of **15** was complete within the duration of the laser pulse. The rearrangement of derivatives of **5** to intermediary diazo compounds has recently been employed in a new heterocycle synthesis.[11]

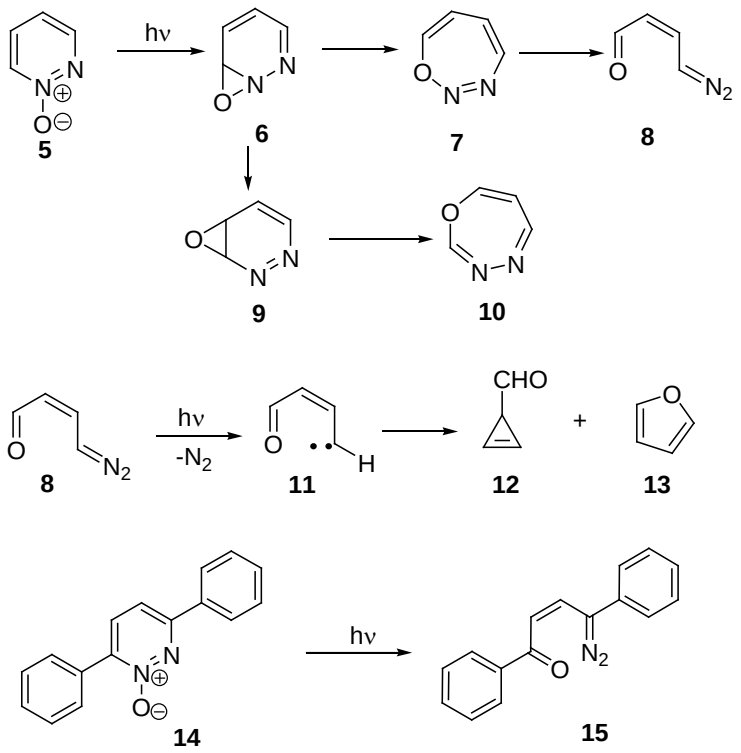

Scheme 2. Photochemical reactions of **5** and **14**

In this contribution, we wish to report on the observation of transient intermediates in the photochemistry of pyridazine *N*-oxide **5**, using picosecond time-resolved resonance Raman spectroscopy (ps-TR^3), femtosecond time-resolved transient absorption (fs-TA), nanosecond time-resolved transient absorption (ns-TA), nanosecond time-resolved IR (ns-IR) and nanosecond time-resolved resonance Raman (ns-TR^3) spectroscopies. We also present the results of DFT and *ab initio* studies concerning possible intermediates in the reaction examined.

Results and Discussion

Experimental results

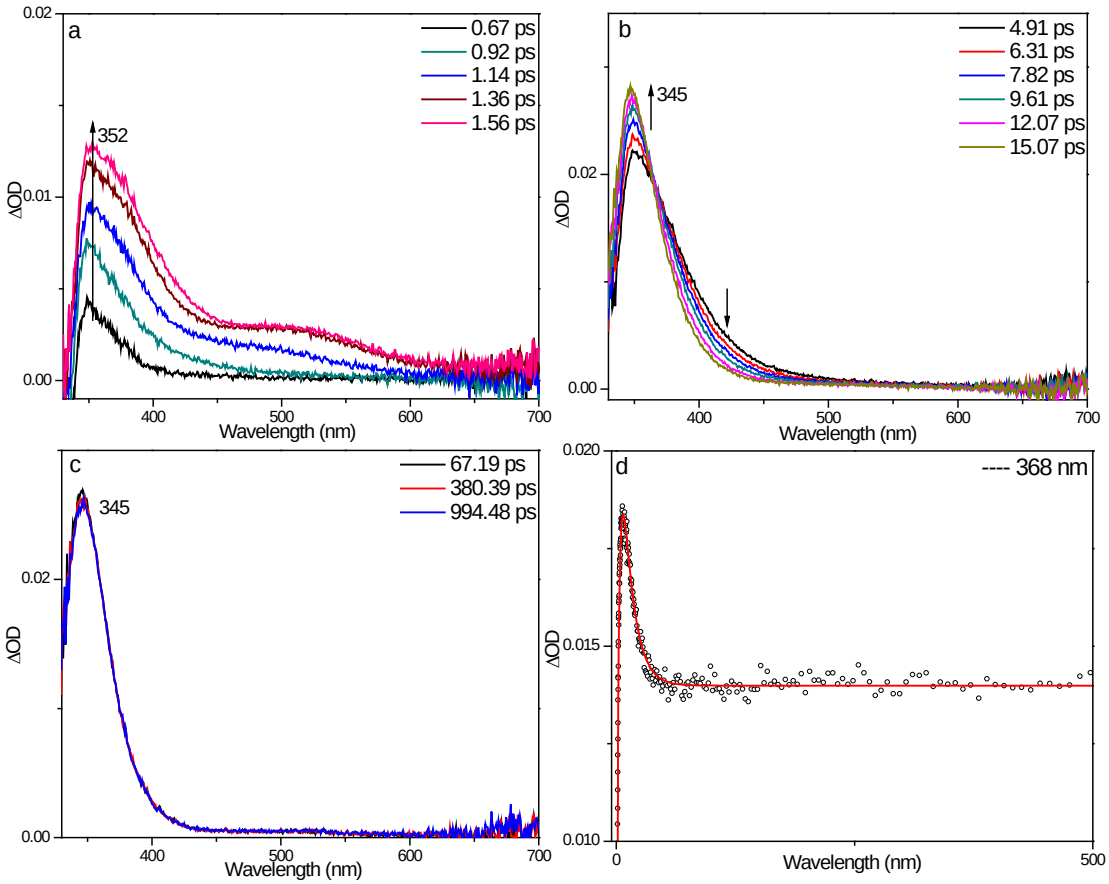

Figure 1. (a, b and c) The fs-TA spectra of **5** in acetonitrile upon 266 nm irradiation. (d) The kinetic of the fs-TA bands observed at 368 nm. The solid lines indicate the kinetics fitting to the experimental data points.

Figure 1 displays the fs-TA spectra of **5** in acetonitrile. The spectra change at the early delay time within 1.56 ps is assigned as the internal conversion (IC) process from S_n to S_1. Then, the S_1 of **5** quickly converts into another species absorbing at 345 nm (denoted as IM1) with an isosbestic point at 365 nm. After the complete generation of this new species, its absorbance stays constant up to around 1 ns. The kinetics at 345 nm was fit by a function with an exponential rise of 2.67 ps (A_1=-0.012) and an exponential decay of 11.36 ps (A_2=0.009). The short-lived time constant is consistent with a typical IC process and the relatively longer time constant corresponds to the growth time constant of IM1.

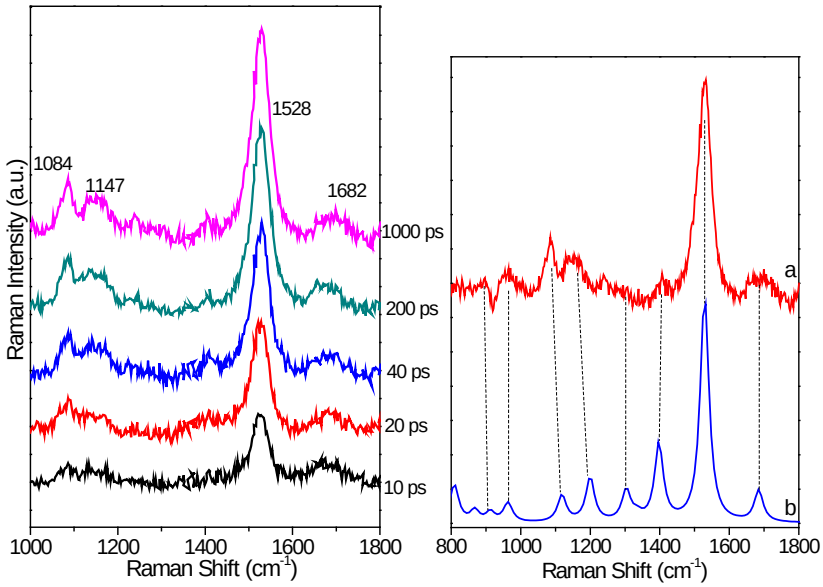

Figure 2. (Left) The ps-TR^3 spectra of **5** in acetonitrile recorded with 266 nm pump wavelength and 365 nm probe wavelength. (Right) Comparison of (a) the experimental ps-TR^3 of **5** recorded at 1000 ps with (b) the M06/cc-pVTZ-calculated Raman spectrum (using a scaled factor of 0.978) of the species **6**.

To gain structural information for the species IM1 formed on the tens of ps time scale and help better understand the photophysical and photochemical processes of **5** in acetonitrile, ps-TR^3 experiments were conducted for **5** and these results are given in Figure 2. Examination of Figure 2 suggests that mainly one species was generated at very early time and grew in as the delay time between the pump and the probe lasers increased. As this species was probed upon irradiation, we tentatively assigned it as the species **6** (1,2-diaza-7-oxa-bicyclo[4.1.0]hepta-2,4-diene) which is produced after the irradiation of **5**, as suggested in Scheme 2. Therefore, the experimental ps-TR^3 spectrum was compared with the DFT simulated Raman spectrum of **6** (see Figure 2 right). The excellent agreement between the experimental and the calculated vibrational frequency patterns provides evidence for the assignment of the species detected in ps-TR^3 to **6**. Considering the generation during the same delay time period, it is reasonable to assume the species IM1 in fs-TA is also **6**.

Nanosecond laser flash photolysis (λ_{exc} = 308 nm) of **5** in acetonitrile solution at T = 294 K led to the detection of two transient intermediates. The first transient (λ_{max} = 390 nm) decayed with a lifetime of τ ~ 900 ns (first order kinetics), while the second transient (λ_{max} = 340 nm) grew in with an identical lifetime (Figure 3). As the spectrum exhibits an isosbestic point at λ ~ 370 nm (Figure 4), this picture is consistent with only one transient being formed initially, which subsequently decays to form the second transient. It is noted that due to partial overlap

of the bands of the decaying and the growing transient, the real absorption maxima of the transient species may differ from the ones observed experimentally. In addition, we also observed "instantaneous" product formation (λ_{max} = 350 nm), which was too rapid to be resolved with our experimental set-up, thus complicating the mechanistic scheme. We note that the growing transient is stable on the longest time-scales accessible to the nanosecond equipment used, which points to it being a compound of at least millisecond lifetime.

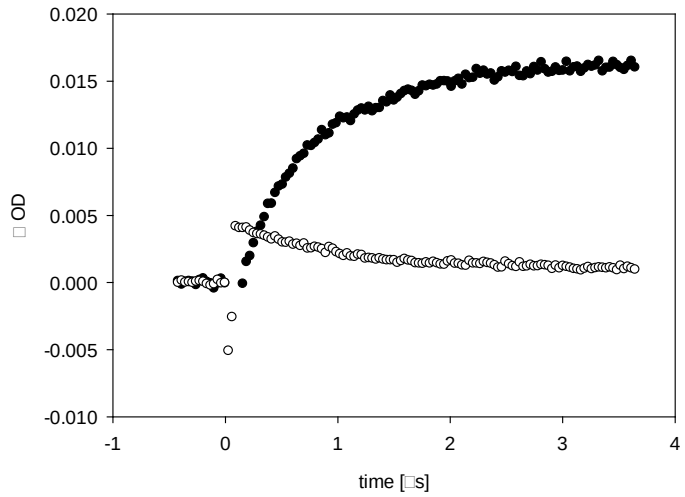

Figure 3. Traces recorded after photolysis (308 nm) of **5** in acetonitrile. Monitoring wavelength is 315 nm (growing species, diazo compound **8**) and 400 nm (decaying species).

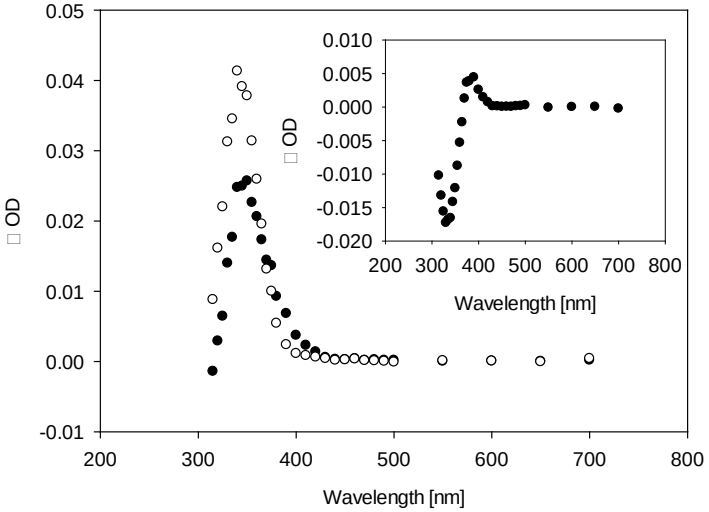

Figure 4. ns-TA spectra (λ_{exc} = 308 nm) of **5** in acetonitrile. Dark circles: spectrum recorded at 200 ns. Light circles: spectrum recorded at 3 μs. Inset: difference spectrum (200 ns – 3 μs).

Neither growth nor decay were affected by purging the solution with oxygen or adding 0.2 % 1-octene, which essentially rules out any participation of triplet excited states or highly

oxidizing species such as O (^{3}P). This makes it likely that the reaction observed corresponds to an intramolecular rearrangement taking place on the ground state singlet surface. A study of the temperature dependence of the rearrangement (in acetonitrile) yielded a linear Arrhenius plot (Figure 5), with the resulting parameters log (A / s^{-1}) = 11.3 $\pm$ 0.5 and E_a = (7.1 $\pm$ 0.5) kcal mol^{-1}.

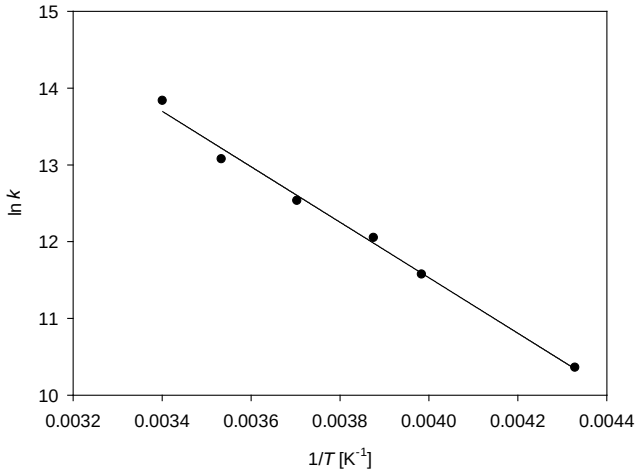

Figure 5. Arrhenius plot (T = 230 – 294 K) for the formation of diazo compound **8** (λ_{mon} = 345 nm, λ_{exc} = 308 nm).

Similar observations were made using $CFCl_3$ as solvent. At ambient temperature, again the decay at λ = 400 nm with synchronous growth at λ = 345 nm was observed, τ being ca. 700 ns.

Product studies on the photochemistry of **5** had revealed the formation of carbene-derived products such as cyclopropene-3-carbaldehyde or furan, thus suggesting the intermediacy of diazo compound **8**. The diazo-chromophore usually exhibits very strong and diagnostic IR bands between 2000 and 2150 cm^{-1}, which makes the photorearrangement of **5** an ideal candidate to be studied with the time-resolved IR spectroscopy.

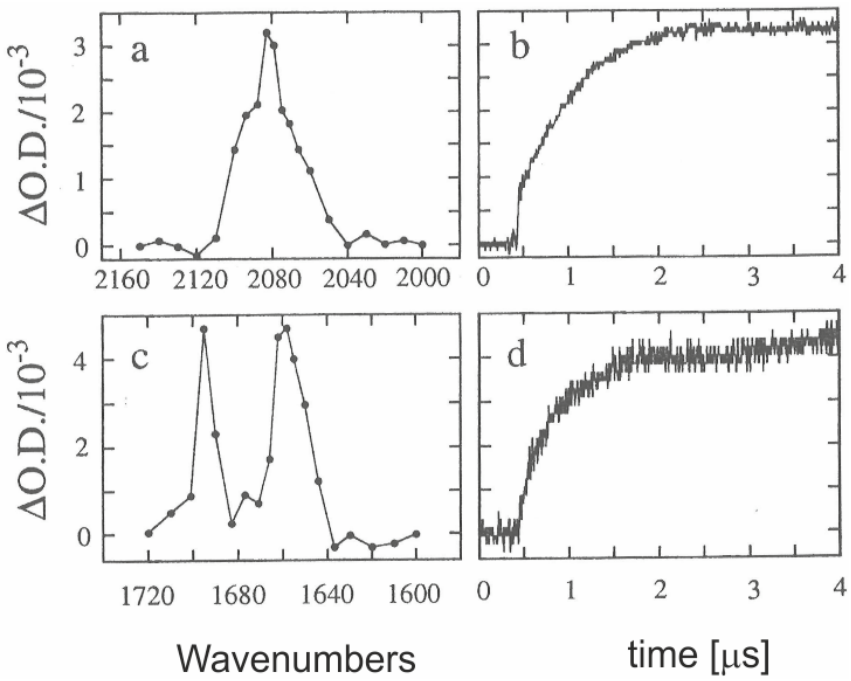

Figure 6. (a) and (c) ns-IR spectrum observed at 2 μs after photolysis (308 nm) of **5** in CCl_4. (b) Transient trace monitored at 2079 cm^{-1}. (d) Transient trace monitored at 1696 cm^{-1}.

Indeed, upon photolysis (λ_{exc} = 308 nm, CCl_4) of **5** we were able to monitor the growth of an IR band with a maximum at 2079 cm^{-1} (Figure 6). Further IR bands observed at 1696 and 1659 cm^{-1} can be assigned to the C=O and the C=C stretching in **8**. Carbonyl- and C=C-stretching frequencies in this range are typical of conjugated aldehydes. Hence we can confidently assign diazo compound **8** to be the product growing in at ambient temperature. Unfortunately we were unable to detect any IR absorptions due to a decaying species, which is not particularly surprising in view of the much lower IR-intensities to be expected for the bands of any of the cyclic precursor molecules to **8**.

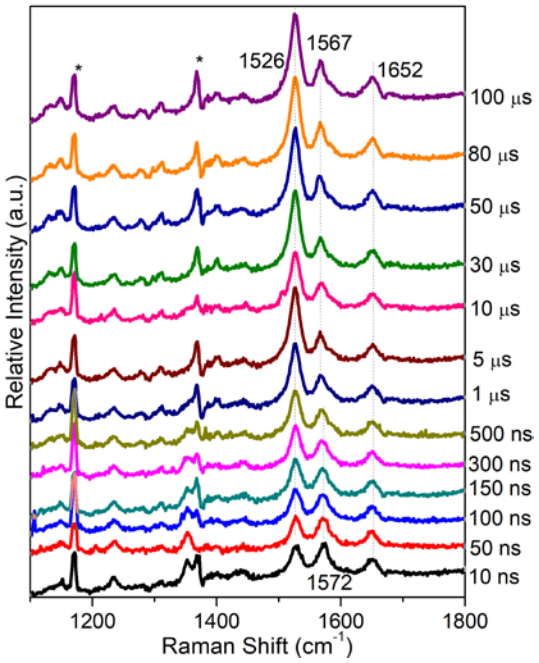

Figure 7. The ns-TR^3 spectra of **5** in acetonitrile recorded using a 266 nm pump wavelength and a 355 nm probe wavelength. The asterisk (*) marks regions affected by solvent subtraction artifacts and/or stray light.

Two species are detected for **5** in acetonitrile in ns-TR^3 experiments (Figure 7). The first one appears upon irradiation and lasts for till the detection limitation (100 μs). The second species was detected from 150 ns as suggested by the increasement of the peak intensity at 1526 cm^{-1}. As the two species coexisted with several overlapped Raman features, the Raman signal at 10 ns was substracted from the one recorded at 100 μs to gain the Raman spectrum for the second species and the subtracted result was given in Figure 8 (a). Considering the very stable character of the second species, we compared its Raman spectrum with the calculated one for the final ring-opening product **8** (Figure 8 b). The reasonable similarities between the experimental and the calculated Raman spectra suggests the second species probed in the ns-TR^3 experiments is **8**.

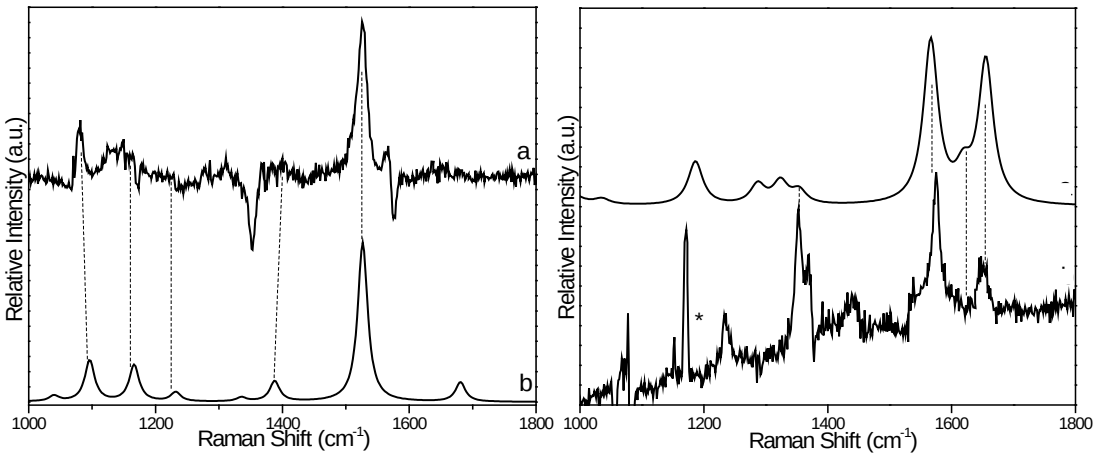

Figure 8. Comparison of (a) the experimental ns-TR^3 spectrum remaining after subtraction of an appropriately scaled spectrum at 10 ns from the spectrum recorded at 100 μs with (b) the simulated Raman spectra of diazo compound **8** (M06/6-31G*, scaling factor is 0.935, half-width is 10), and comparison of (c) the simulated Raman spectra of diazoxepine **10** (see its structure in Scheme 2) (M06/cc-pVTZ, scaling factor is 0.965, half-width is 15) with (d) the experimental ns-TR^3 spectrum remaining after subtraction of an appropriately scaled spectrum in Figure 8a from the spectrum recorded at 10 ns. The asterisk (*) marks regions affected by solvent subtraction artifacts and/or stray light.

Then, an appropriately scaled spectrum in Figure 8 (a) was subtracted from the spectrum recorded at 10 ns to gain the Raman signal of the first species and the remaining bands after subtraction is given in Figure 8 (d). To assign this species, the Raman spectra for all the possible intermediates and transient species produced between the species **6** with the generation of **8** were simulated and compared with Figure 8 (d). Based on a comparison of calculated and experimental Raman spectra, the transient was assigned to diazoxepine **10** (c.f. Scheme 2). On a timescale up to 100 μs, we did not observe any decay of the bands assigned to **10**, meaning that **10** is a stable product and therefore cannot be the precursor to diazo compound **8**. During the first few ten to few hundred ns, we could observe a very weak signal at 1528 cm^{-1} (the wavelength of the most intense Raman band of **6**), on top of the much more intense and growing band of **8** with a maximum at 1526 cm^{-1} (see Figure S1, Supporting Information). The very small signal intensity and the overlap with a more intense band of **8**, however, prevents us from accurately determining the lifetime of this decaying transient. Nevertheless, it allows us to cautiously state that **6** likely has a decay lifetime of the order of hundreds of ns, in agreement with the data shown in Figures 1, 4 and 7.

Calculation Results

In order to identify the transient species observed, we performed geometry optimizations on reactive intermediates along the reaction coordinates connecting **5** and **8**, along with transition states connecting the minima. Geometry optimizations were performed employing a variety of DFT methods, RHF theory, 2nd, 3rd, and 4th order Møller-Plesset perturbation theory, and coupled cluster theory with single and double excitations (CCSD) as well as single and double excitations plus perturbational treatment of triple excitations (CCSD(T)). In addition to the single reference methods, we also employed a multireference method (CASSCF with 8,8 active space). On selected levels of theory, calculations were also done employing a polarizable continuum model to account for solvation by acetonitrile, and carbon tetrachloride (as a model solvent for the very similar $CFCl_3$).

For a consistent picture, the findings of the experimental work – laser photolysis of **5** yielding diazo compound **8** (identified *via* ns-IR and ns-TR[3]), with the bicyclic oxaziridine **6** as an intermediate (as identified by ps-TR[3]) need to reflect the results of the computational work. However, it turned out that **6**, **7**, and the transition states (TS) connecting **6** and **7** as well as **7** and **8** are extremely challenging stationary points to correctly describe by quantum chemical methods. In many cases either **7** or **6** and **7** were not predicted to be minimum structures, and the stabilities of **6** and **7** diverged widely depending on the method chosen.

Table S1 (see Supporting Information) provides a summary of the energies obtained in our geometry optimizations. To summarize the results presented in Table S1, we can state that the barriers predicted for the decay of **6** and **7** diverge significantly. Many methods, like MP2 or B3LYP, fail to provide a minimum structure for both **6** and **7**. Other methods, like the Minnesota functionals employed, CCSD or CCSD(T), give a minimum structure for **6**, but not for **7**. Only a few methods (RHF, CASSCF, and MP3) also find **7** to be a stationary point on the potential energy surface.[12] However, even with the methods commonly accepted to be highly accurate, like CCSD and CCSD(T), the barrier for decay of **6** is underestimated significantly (CCSD: 2.8 kcal mol^{-1}; CCSD(T): 0.4 kcal mol^{-1}; experiment: 7.1 kcal mol^{-1}), and DFT methods normally believed to give fairly accurate thermochemical data, like M06, while providing Raman spectra in excellent agreement with the experimental TR[3] spectra of **6** (and hence likely very good calculated geometries), fail completely in predicting the stability of **6**. The fact that the CASSCF(8,8) results closely mirror the results obtained by Hartree-Fock theory suggests that the problems should not be due to the system having significant multireference character. This conclusion is also supported by the observation that in CCSD(T) calculations the values of the T_1 diagnostic[13] always were well below 0.02.

However, unlike static electron correlation, the degree of dynamic electron correlation does play a large role in determining the stability of **6** and **7**. The general trend observed is that without dynamic electron correlation included (HF and CASSCF), the barriers for decay of **6** and **7** are highest. Adding solvation by acetonitrile or carbon tetrachloride via a polarizable continuum model generally stabilizes both **6** and **7**, albeit not by much. Adding explicit solvent molecules also has little influence – at the M06/6-31G(d) level of theory, **7** is not a minimum structure, if the compound is placed in a cluster of twelve molecules of either CH_3CN or CCl_4. The electronic energy of activation for ring opening of **6** in a cluster of twelve molecules of CCl_4 is calculated (M06/6-31G(d)) as ΔU = 0.3 kcal mol^{-1}, and therefore is of a similar order of magnitude as that of the same reaction in the gas phase. Inclusion of some dynamic electron correlation (as in MP2) leads to destabilization of **6** and **7** to a degree that they are no longer minima, and only use of highly correlated methods recovers some stability at least for **6**. In the series of calculations employing Møller-Plesset perturbation theory, the trends observed are not linear, however, and a maximum of stability is reached for both **6** and **7** when MP3 theory is employed. While this gave us the opportunity to calculate the Raman spectrum of **7** at a post-HF level of theory, the situation clearly is unsatisfactory from the standpoint of a computational chemist.

Figure 9 shows the optimized geometries of **6**, **7** and the TS connecting them and **8**. Relevant geometric parameters are listed for MP3/cc-pVTZ, M06/cc-pVTZ, CCSD/cc-pVTZ, and CCSD(T)/cc-pVTZ.

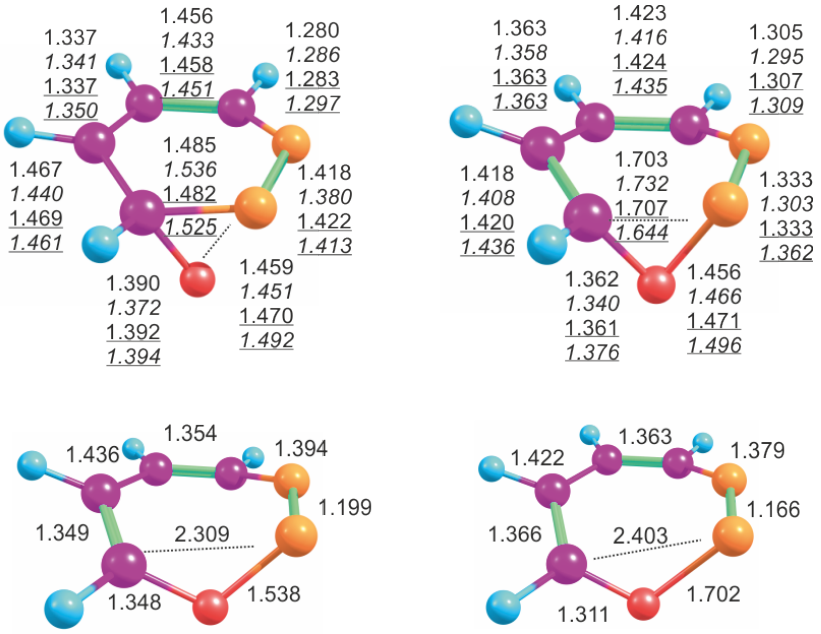

Figure 9. Optimized geometries for **6** (top left), TS **6** → **7** (top right), **7** (bottom left), and TS **7** → **8** (bottom right). Selected geometric parameters: normal font: MP3/cc-pVTZ. Italics: M06/cc-pVTZ. Underlined: CCSD/cc-pVTZ. Underlined italics: CCSD(T)/cc-pVTZ.

The results show that for **6** and the TS **6** → **7**, the results depend very critically on the level of theory used for optimization. While there is good agreement between the results obtained at the MP3 and CCSD levels of theory, CCSD(T) optimization leads to a far earlier TS than any other method (TS **6** → **7**: CCSD(T): $R_{C\text{-}N}$ = 1.644 Å; CCSD: $R_{C\text{-}N}$ = 1.707 Å), which is in line with the very small barrier (electronic energy of activation 0.4 kcal mol^{-1}) calculated at the CCSD(T) level of theory. In case of the reaction **7** → **8**, where calculated post-HF data is only available for the MP3 method, the calculations indicate a very early TS for ring opening, with a fairly short N-O distance (MP3/cc-pVTZ: $R_{N\text{-}O}$ = 1.702 Å). We have calculated (B3LYP/6-311G(d)//M06/cc-pVTZ or B3LYP/6-311G(d)//MP3/cc-pVTZ) the NICS[14] values for **6**, **7**, TS **6**/**7**, and TS **7**/**8** (1 Å above the plane of the rings). They are obtained as δ = -5.8 (**6**), -13.7 (TS **6**/**7**), -7.4 (**7**), and -7.5 ppm (TS **7**/**8**). Hence, at least the TS for the electrocyclic ring opening reaction of **6** can be characterized as distinctly (homo)aromatic, and all other stationary points also bear a weak aromatic character.

In principle, oxaziridine **6** can also undergo an oxygen walk rearrangement to yield oxirane **9**, which could then undergo an electrocyclic ring opening to give oxadiazepine **10** (see Scheme 2). The barrier calculated for the reaction **6** → **9** is significant, ruling out that this reaction would happen on the ground state hypersurface. However, species **9**/**10** could also be formed directly on the excited state hypersurface, possibly via a conical intersection of similar geometry as the TS of the ground-state oxygen walk rearrangement. Such biradical-type structures have previously been postulated for a related system.[6] We have optimized (M06/cc-pVTZ and MP3/cc-pVTZ) the stationary points along the reaction coordinate **6** → **9** → **10**, and find that the barrier for the oxygen walk rearrangement **6** → **9** far exceeds the very small barrier for the electrocyclic ring opening **6** → **7** (**8**). Oxirane **9**, once formed, should undergo an extremely rapid electrocyclic ring opening reaction, yielding 1,3,4-oxadiazepine **10** with a very small barrier of $\Delta H^{\ddagger}$ = 0.4 kcal mol^{-1} (MP3: 2.5 kcal mol^{-1}). The latter species **10**, on the other hand, is predicted to be very stable. A TS for the rearrangement of **9** to diazo compound **8** could be localized, but the barrier is prohibitively high ($\Delta H^{\ddagger}$ = 30.7 kcal mol^{-1} (M06) from **10** via **9**). An alternative ring opening reaction to yield singlet carbene **16**, which is calculated to have a vibrational spectrum very similar to **8**, is predicted to be significantly endothermic.

Figure 10 shows calculated enthalpies of the stationary points along the reaction coordinate involving **9** and **10**. For optimized geometries please see the SI.

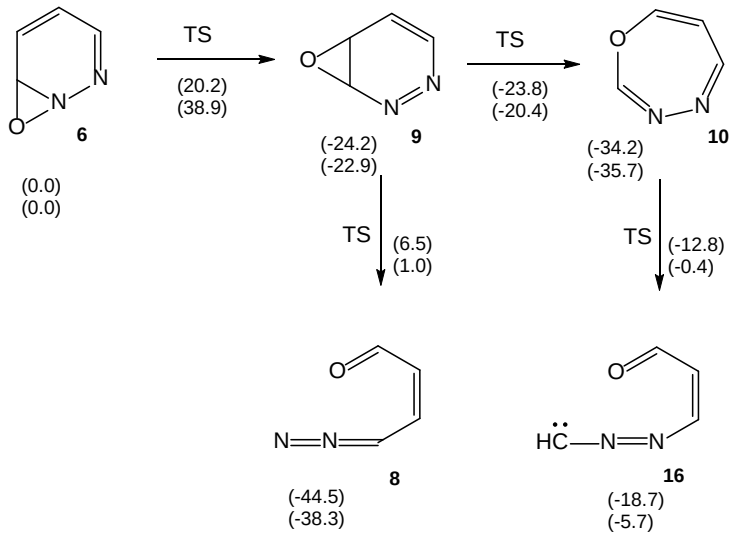

Figure 10. Enthalpies (kcal mol^{-1}) (normal font: M06/cc-pVTZ; underlined: MP3/cc-pVTZ) of stationary points related to the reaction coordinates **6** → **9** → **10** → **16**. Please note that the (very facile) formation of **8** via **7** has been omitted in this Figure.

We note that calculations indicate that correlated *ab initio* calculations on **9** / **10** result in similar trends as observed for calculations on **6** and **7**. Thus, employing MP2/cc-pVTZ, **9** was not found to be a minimum structure, whereas the stability of **10** towards ring-opening to **16** was calculated to be very similar to the result using M06/cc-pVTZ (MP2: $\Delta H^{\ddagger}$ = 22.8 kcal mol^{-1}; M06: $\Delta H^{\ddagger}$ = 21.4 kcal mol^{-1}). MP3 theory, on the other hand, largely confirmed the results obtained by M06, with a small barrier for the electrocyclic ring opening reaction **9** → **10**.

Conclusion

Photolysis of pyridazine *N*-oxide **5** yields three rearrangement products. TR^3 measurements in combination with calculated Raman spectra allow for the clear identification of the short-lived transient as oxaziridine **6**, formed via the S_1 state of **5**. Oxaziridine **6** decays to diazo compound **8** on a timescale of hundreds of nanoseconds. A second species observed in the ns-TR^3 experiments is assigned to 1,3,4-oxadiazepine **10**, which is stable on the timescale of our experiment. Seven-membered ring **10** is formed via the very short-lived oxirane **9** (not observed), which in turn likely is formed from the S_1 state of **5** via a conical intersection resembling the TS of the oxygen walk rearrangement **6** → **9**. The results presented raise

several important issues. Firstly, the experimentally determined activation energy for decay of **6** (7.1 $\pm$ 0.5 kcal mol^{-1}) is far higher than the barrier calculated for this reaction, with any of the methods employed that include dynamic electron correlation. Secondly, a series of geometry optimizations on the electrocyclic ring-opening of oxaziridine **6**, using increasingly higher correlated methods, also indicate that no convergence had been reached (both in terms of geometries of **6** and TS **6**/**7**, and in terms of activation energies), even when employing a CCSD(T) optimization. This divergence observed in the properties of **6** leads us to believe that the description of **7** at the same levels of theory, **7** by most methods not being predicted to be a stationary point, might also be flawed. We therefore suggest that the stationary points along the reaction coordinate **6** $\rightarrow$ **7** $\rightarrow$ **8** represent excellent and challenging candidate molecules for theoretical chemists and method developers to fine-tune their computational methodology, as methods beyond CCSD(T), such as CCSDT(Q), currently are far too demanding in terms of CPU time and memory requirements to be feasible for systems such as **6** and **7**, at least as far as geometry optimizations are concerned.

Experimental

Pyridazine *N*-oxide **5** was synthesized according to a literature procedure[15] or obtained from Aldrich. Triethylphosphite (Kodak Eastman) was freshly distilled prior to use. Acetonitrile (BDH Omnisolv) was used as received; fluorotrichloromethane (freon 11, Aldrich) was passed twice over an alumina column.

Laser Flash Photolysis with UV/Vis detection (University of Ottawa): The LFP system employed in this study has been described in previous publications.[16] **5** was photolyzed using a Lumonics EX-510 excimer laser operated with Xe/HCl/Ne (308 nm, ca. 5 ns, ca. 100 mJ / pulse). As **5** is rapidly depleted upon LFP, a rapid flow of fresh sample solution had to be maintained during experiments.

Time-Resolved Infrared (TRIR) Experiments (NRC, Ottawa): Solutions for the TRIR measurements (prepared to give an optical density of 0.3 at 308 nm) were flowed through a 1 mm path length CaF_2 cell. The excitation source was a Lumonics Excimer-500 laser (XeCl; 308 nm; 10 ns pulse width); the IR probe source was a Mutek Model MPS-1000 diode laser (1540 – 2280 cm^{-1}). Kinetic traces at a particular IR frequency were obtained by measuring the IR intensity through the sample before, during, and after absorption of the UV laser pulse. The response time of the detector was ca. 250 ns. Absorption of the excitation pulse caused a shockwave in the kinetic traces, which was dependent on the solution and path length. All kinetic traces were therefore corrected by subtracting the shockwave measured at an IR

frequency at which no transient was observed. Spectra were obtained by measuring the individual kinetic traces at 4 – 10 cm^{-1} increments throughout the region of interest, and plotting Δ OD vs. wavenumber for a fixed time after the 308 nm pulse. Full details of the TRIR system have been given elsewhere.[17]

ps-TR^3 and ns-TR^3 Experiments: The ps-TR^3 and ns-TR^3 experiments were performed in our lab at the University of Hong Kong with the methods described previously,[18] and a short description is given. A 266 nm pump wavelength and a 365 nm probe wavelength were used in the ps-TR^3 experiments. A 266 nm pump wavelength and the 355 nm probe wavelength were used in the ns-TR^3 experiments. Sample concentrations were $\sim 5 \times 10^{-4}$ M.

Calculations: All calculations were performed using the *Gaussian 09* suite of programs,[19] except for the CCSD and CCSD(T) geometry optimizations, and the calculation of the MP3 Raman spectra, which were performed employing ORCA Vers. 3.[20] All minima and transition states except the stationary points optimized at the CCSD(T)/cc-pVTZ level of theory were characterized as such by performing a vibrational analysis. The effects of solvation were accounted for by employing a polarizable continuum model (scrf=pcm).[21,22] Calculations were performed using the B3LYP,[23] M06,[24] and M06-2X,[25] functionals, Hartree-Fock theory,[25] second-order,[26] third-order,[27] and fourth-order Møller-Plesset perturbation theory,[28] coupled-cluster theory with single and double excitations (CCSD),[29] and coupled cluster theory with single and double excitations with perturbational treatment of triple excitations (CCSD(T)).[30] As a multireference method, CASSCF[31] was employed, using an active space of eight electrons in eight orbitals (CASSCF(8,8)). Basis sets used include the standard 6-31G(d)[32] and cc-pVTZ[33] basis sets.

Acknowledgement

GB thanks the EPSRC UK National Service for Computational Chemistry Software (NSCCS) for a CPU time grant. The initial work on this project (University of Ottawa) had been supported by a NATO scholarship for GB, which is gratefully acknowledged. DLP acknowledges support from the University of Hong Kong Development Fund 2013-2014 project "New Ultrafast Spectroscopy Experiments for Shared Facilities". We gratefully acknowledge the support of Dr. Janusz Lusztyk (Steacie Institute for Molecular Sciences, NRC, Ottawa) and of Prof. J. C. Scaiano (Department of Chemistry, University of Ottawa).

Supporting information available

Experimental ns-TR3 spectra observed after different time intervals after laser excitation of **5**.
Table S1 listing the absolute electronic energies and relative electronic energies of stationary points in the reaction sequence **6** → **7** → **8**, obtained by various methods. Electronic energies of stationary points in the reaction coordinates involving **6**, **8** , **9**, **10**, **16**. A .xyz file containing the geometries of all stationary points optimized.

References

1) Albini, A.; Alpegiani, M. The Photochemistry of the *N*-Oxide Function. *Chem. Rev.* **1984**, *84*, 43-71. DOI: 10.1021/cr00059a004
2) Albini, A.; Fagnoni, M. *Photochemistry of N-Oxides*. in CRC Handbook of Photochemistry, 2nd Edition, CRC Press, Boca Raton, Fl, 2004.
3) Bucher, G.; Scaiano, J. C. Laser Flash Photolysis of Pyridine *N*-Oxide: Kinetic Studies of Atomic Oxygen [O(^{3}P)] in Solution. *J. Phys. Chem.* **1994**, *98*, 12471-12473. DOI: 10.1021/j100099a004
4) Buchardt, O.; Christensen, J. J.; Nielsen, P. E.; Koganty, R. R.; Finsen, L.; Lohse, C.; Becher, J. Photochemical Studies. XXII. Photochemical Ring-Opening of Pyridine *N*-Oxide to 5-Oxo-2-Pentenenitrile and / or 5-Oxo-3-Pentenenitrile. A Reassignment of Structure. *Acta Chem. Scand.* **1980**, *34b*, 31-39. DOI: 10.3891/acta.chem.scand.34b-0031
5) Finsen, L.; Becher, J.; Buchardt, O.; Koganty, R. R. Derivatives and Reactions of Glutaconaldehyde. XI. N-Substituted 5-Amino-2,4-Pentadienenals, their Oximes, and 5-Amino-2,4-Pentadienenitriles. Structural Analysis by ^{1}H and ^{13}C NMR Spectroscopy. *Acta Chem. Scand.* **1980**, *34b*, 513-518. DOI: 10.3891/acta.chem.scand.34b-0513
6) Albini, A.; Fasani, E.; Frattini, V. Medium and Substituent Effects on the Photochemistry of Phenanthridine *N*-Oxides. Is An Intermediate of Diradical Character Involved in the Photorearrangement of Heterocyclic *N*-oxides? *J. Chem. Soc. Perkin Trans.* **1988**, *2*, 235-240. DOI: 10.1039/P29880000235
7) Lohse, C.; Hagedorn, L.; Albini, A.; Fasani, E. Photochemistry of Pyridine *N*-oxides. *Tetrahedron* **1988**, *44*, 2591-2600. DOI: 10.1016/S0040-4020(01)81710-5
8) Albini, A.; Fasani, E.; Lohse, C. Photochemistry of Pyridine *N*-Oxides. Trapping of An Intermediate with Amines. *Heterocycles*. **1988**, *27*, 113-123. DOI: 10.3987/COM-87-4267

9) Tsuchiya, T.; Arai, H.; Igeta, H. Photolysis of Pyridazine *N*-Oxides; Formation of Cyclopropenyl Ketones. *J. Chem. Soc. Chem. Comm.* **1972**, 550-551. DOI: 10.1039/C39720000550

10) Tomer, K. B.; Harrit, N.; Rosenthal, I.; Buchardt, O.; Kumler, P. L.; Creed, D. Photochemical Studies. XX. Photochemical Behavior of Aromatic 1,2-Diazine *N*-Oxides. *J. Am. Chem. Soc.* **1973**, *95*, 7402-7406. DOI: 10.1021/ja00803a031

11) Portillo, M.; Maxwell, M. A.; Frederich, J. H. Pyridazine *N*-Oxides as Precursors to Metallocarbenes: Rhodium-Catalyzed Transannulation with Pyrroles. *Org. Lett.* **2016**, *18*, 5142-5145. DOI: 10.1021/acs.orglett.5b03064

12) Subbotina, J. O.; Bakulev, V. A.; Herges, R.; Fabian, W. M. F. 1,7-Cyclization of 1-Diazo-2,4-Pentadiene and Its Heteroanalogues: DFT Study. *Int. J. Quant. Chem.* **2006**, 2229-2235. DOI: 10.1002/qua.20947

13) Lee, T. J.; Taylor, P. R. A Diagnostic for Determining the Quality of Single-Reference Electron Correlation Methods. *Int. J. Quantum Chem., Quant. Chem. Symp.* **1989**, *36*, 199-207.

14) Schleyer, P. v. R.; Maerker, C.; Dransfeld, A.; Jiao, H.; v. Eikema Hommes, N. J. R. Nucleus-Independent Chemical Shifts: A Simple and Efficient Aromaticity Probe. *J. Am. Chem. Soc.* **1996**, *118*, 6317-6318. DOI: 10.1021/ja960582d

15) Koelsch, C. F.; Gumprecht, W. H. Some Diazine-*N*-Oxides. *J. Org. Chem.* **1958**, *23*, 1603-1606. DOI: 10.1021/jo01105a003

16) Scaiano, J. C.; Tanner, M.; Weir, D. Exploratory Study of the Intermolecular Reactivity of Excited Diphenylmethyl Radicals. *J. Am. Chem. Soc.* **1985**, *107*, 4396-4403. DOI: 10.1021/ja00301a005

17) (a) Rayner, D.M.; Nazran, A.S.; Drouin, M; Hackett, P.A. 248 nm Photolysis of Tricarbonylnitrosylcobalt. *J. Phys. Chem.* **1986**, *90*, 2882-2888; (b) Wagner, B.D.; Arnold, B.R.; Brown, G.S.; Lusztyk, J. Spectroscopy and Absolute Reactivity of Ketenes in Acetonitrile Studied by Laser Flash Photolysis with Time-Resolved Infrared Detection. *J. Am. Chem. Soc.* **1998**, *120*, 1827-1834.

18) (a) Ma, C.; Kwok, M. W.; Chan, W. S.; Du, Y.; Kan, J. T. W.; Toy, P. H.; Phillips, D. L. Ultrafast Time-Resolved Transient Absorption and Resonance Raman Spectroscopy Study of the Photodeprotection and Rearrangement Reactions of *p*-Hydroxyphenacyl Caged Phosphates. *J. Am. Chem. Soc*. **2006**, *128*, 2558-2570. DOI: 10.1021/ja0532032; (b) Ma, J.; Su, T.; Li, M.-D.; Du, W.; Huang, J.; Guan, X.; Phillips, D. L. How and When Does an Unusual and Efficient Photoredox Reaction of

2–(1-Hydroxyethyl) 9,10-Anthraquinone Occur? A Combined Time-Resolved Spectroscopic and DFT Study. *J. Am. Chem. Soc.* **2012**, *134*, 14858-14868. DOI: 10.1021/ja304441n

19) Gaussian 09, Revision A.02, Frisch, M. J.; Trucks, G. W.; Schlegel, H. B.; Scuseria, G. E.; Robb, M. A.; Cheeseman, J. R.; Scalmani, G.; Barone, V.; Mennucci, B.; Petersson, G. A.; Nakatsuji, H.; Caricato, M.; Li, X.; Hratchian, H. P.; Izmaylov, A. F.; Bloino, J.; Zheng, G.; Sonnenberg, J. L.; Hada, M.; Ehara, M.; Toyota, K.; Fukuda, R.; Hasegawa, J.; Ishida, M.; Nakajima, T.; Honda, Y.; Kitao, O.; Nakai, H.; Vreven, T.; Montgomery, J. A., Jr.; Peralta, J. E.; Ogliaro, F.; Bearpark, M.; Heyd, J. J.; Brothers, E.; Kudin, K. N.; Staroverov, V. N.; Kobayashi, R.; Normand, J.; Raghavachari, K.; Rendell, A.; Burant, J. C.; Iyengar, S. S.; Tomasi, J.; Cossi, M.; Rega, N.; Millam, J. M.; Klene, M.; Knox, J. E.; Cross, J. B.; Bakken, V.; Adamo, C.; Jaramillo, J.; Gomperts, R.; Stratmann, R. E.; Yazyev, O.; Austin, A. J.; Cammi, R.; Pomelli, C.; Ochterski, J. W.; Martin, R. L.; Morokuma, K.; Zakrzewski, V. G.; Voth, G. A.; Salvador, P.; Dannenberg, J. J.; Dapprich, S.; Daniels, A. D.; Farkas, Ö.; Foresman, J. B.; Ortiz, J. V.; Cioslowski, J.; Fox, D. J. Gaussian, Inc., Wallingford CT, **2009**.

20) Neese, F. The ORCA Program System. *Wiley Interdiscip. Rev.: Comput. Mol. Sci.* **2012**, *2*, 73-78. DOI: 10.1002/wcms.81

21) Tomasi, J.; Mennucci, B.; Cammi, R. Quantum Mechanical Continuum Solvation Models. *Chem. Rev*. **2005**, *105*, 2999-3094. DOI: 10.1021/cr9904009

22) Miertuš, S.; Scrocco, E.; Tomasi, J. Electrostatic Interaction of a Solute with a Continuum. A Direct Utilization of Ab-initio Molecular Potentials for the Prevision of Solvent Effects. *Chem. Phys*. **1981**, *55*, 117-129. DOI: 10.1016/0301-0104(81)85090-2

23) Becke, A. D. Density-Functional Thermochemistry. III. The Role of the Exact Exchange. *J. Chem. Phys*. **1993**, *98*, 5648-5652. DOI: 10.1063/1.464913

24) Zhao, Y.; Truhlar, D. G. The M06 Suite of Density Functionals for Main Group Thermochemistry, Thermochemical Kinetics, Noncovalent Interactions, Excited States, and Transition Elements: Two New Functionals and Systematic Testing of Four M06-class Functionals and 12 Other Functionals. *Theor. Chem. Acc.* **2008**, *120*, 215-241. DOI: 10.1007/s00214-007-0310-x

25) Roothaan, C. C. J. New Developments in Molecular Orbital Theory. *Rev. Mod. Phys.*, **1951**, *23*, 69-89. DOI: 10.1103/RevModPhys.23.69

26) Frisch, M. J.; Head-Gordon, M.; Pople, J. A. Direct MP2 Gradient Method. *Chem. Phys. Lett.* **1990**, *166*, 275-280. DOI: 10.1016/0009-2614(90)80029-D

27) Pople, J. A.; Binkley, J. S.; Seeger, R. Theoretical Models Incorporating Electron Correlation. *Int. J. Quantum Chem.* **1976**, *10*, 1-19. DOI: 10.1002/qua.560100802

28) Raghavachari, K.; Pople, J. A. Approximate 4th-Order Perturbation-Theory of Electron Correlation Energy. *Int. J. Quantum Chem.* **1978**, *14*, 91-100. DOI: 10.1002/qua.560140109

29) Scuseria, G. E.; Janssen, C. L.; Schaefer, H. F., III. An Efficient Reformulation of the Closed-shell Coupled Cluster Single and Double Excitation (CCSD) Equations. *J. Chem. Phys.* **1988**, *89*, 7382-7387. DOI: 10.1063/1.455269

30) Purvis, G. D., III; Bartlett, R. J., A Full Coupled-Cluster Singles and Doubles Model – the Inclusion of Disconnected Triples. *J. Chem. Phys.* **1982**, *76*, 1910-1918. DOI: 10.1063/1.443164

31) Hegarty, D.; Robb, M. A. Application of Unitary Group-Methods to Configuration-Interaction Calculations. *Mol. Phys.* **1979**, *38*, 1795-1812. DOI: 10.1080/00268977900102871

32) Hehre, W. J.; Ditchfield, R.; Pople, J. A. Self-Consistent Molecular Orbital Methods. XII. Further Extensions of Gaussian-Type Basis Sets for Use in Molecular Orbital Studies of Organic Molecules. *J. Chem. Phys.* **1972**, *56*, 2257-2261. DOI: 10.1063/1.1677527

33) Dunning, T. H., Jr. Gaussian Basis Sets for Use in Correlated Molecular Calculations. I. The Atoms Boron Through Neon and Hydrogen. *J. Chem. Phys.* **1989**, *90*, 1007-1023. DOI: 10.1063/1.456153

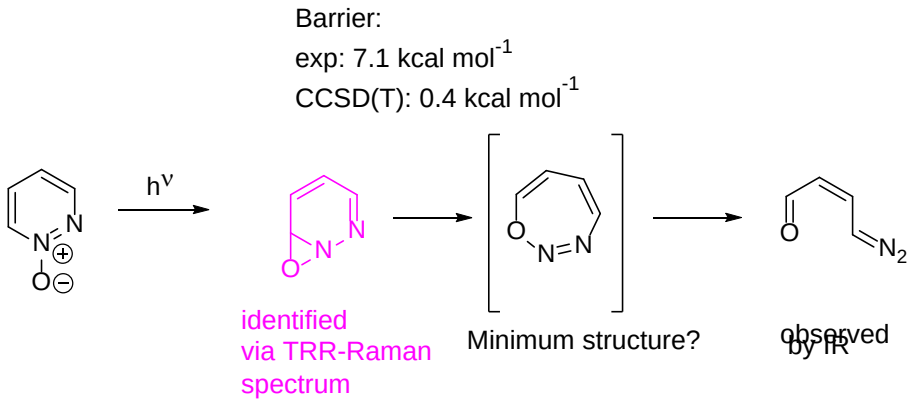

(Graphical abstract only)